

Development of crystalline order during hot-drawing of poly(ethylene terephthalate) film: influence of strain rate*

D. R. Salem

TRI/Princeton, PO Box 625, Princeton, NJ 08542, USA

(Received 13 August 1991; accepted 27 October 1991)

We have studied the evolution of crystalline order during drawing of poly(ethylene terephthalate) at 90°C and at strain rates in the range 0.01–2.1 s⁻¹. The onset of crystallization always occurs at the inflection point in the stress–strain relationship, which shifts to higher strain levels and lower stress levels as strain rate decreases. Crystallinity develops in two regimes: in the low stress regime (regime 1) crystallinity increases more rapidly than in the high stress regime (regime 2). The onset of regime 2 occurs in the region of the sharp upturn in the stress–strain relationship, which shifts to higher strain levels as strain rate decreases, and at a characteristic level of crystallinity, which is independent of strain rate. We suggest that regime 1 involves the formation of a crystallite network which, at the characteristic level of crystallinity, has sufficiently crosslinked and reinforced the polymer that further deformation generates large stresses. WAXS determinations of lateral crystallite dimensions, normal to the 010 and 100 planes, reveal that crystallization in regime 2 involves modest growth of small crystallites (~2.5–3.5 nm), with preferential growth occurring normal to 010. A preliminary investigation of the influence of molecular weight indicates that a lower rate of molecular relaxation at higher molecular weight reduces the strain-rate dependent shift in the onset of crystallization.

(Keywords: poly(ethylene terephthalate); crystallization; stress; strain rate; hot-drawn film)

INTRODUCTION

There have been numerous experimental and theoretical studies of strain-induced crystallization of poly(ethylene terephthalate) (PET)^{1–12} and other flexible chain polymers^{13–24}. Mostly these were concerned with crystallization of oriented, amorphous material by annealing, or of oriented melts by supercooling. Less attention has been devoted to the induction of crystallinity by application of high strains at temperatures above the glass transition. This type of deformation generates large orientation-inducing stresses during crystallization, and is the principal process by which semicrystalline fibres and films of PET are formed.

In the temperature region 80–105°C, which is above the glass transition temperature (T_g) but below the temperature at which thermally induced crystallization becomes significant in unoriented PET, the viscoelastic properties of the amorphous polymer are highly dependent on strain rate $\dot{\epsilon}$ and temperature T , moving from glassy behaviour at low temperatures and high strain rates to rubber-flow behaviour at high temperatures and low strain rates^{10,12,25} (Figure 1). The viscoelastic properties corresponding to a particular combination of temperature and strain rate will influence, in turn, the induction and development of crystallinity during drawing. However, of the studies concerned with structure evolution during drawing of PET in this

temperature region^{10–12,26–34}, only a few have attempted to investigate systematically the effects of varying strain rate and draw temperature^{10–12}. In the work reported here, we examine in detail the influence of strain level, stress level, and strain rate on orientation-induced crystallization and crystal growth in PET film drawn at 90°C.

EXPERIMENTAL

Materials

Details of the undrawn, amorphous PET films used are given in Table 1.

The number average molecular weights were deduced from intrinsic viscosity measurements on the polymer in solution in *o*-chlorophenol, using the \bar{M}_n /intrinsic viscosity relationship of Ravens and Ward³⁵. In most of the work reported here, the Rhône Poulenc film was used; the Goodyear film was used only in the studies of the influence of molecular weight. All the films were of high clarity; they did not contain TiO₂ or other additives.

Deformation

The amorphous film specimen was mounted in the jaws of an Instron tensile tester, and heated to a temperature of 90°C, which took ~20 min. We found that no detectable change in film density occurs during this heat-up period. Immediately after reaching 90°C, the film was drawn at the selected extension rate. At a given extension rate, the load–extension curves for the various draw ratios investigated could be almost exactly

*An abbreviated version of this paper was presented at Speciality Polymers '90, 8–10 August 1990, The Johns Hopkins University, Baltimore, MD, USA

0032-3861/92/153182-07

© 1992 Butterworth-Heinemann Ltd.

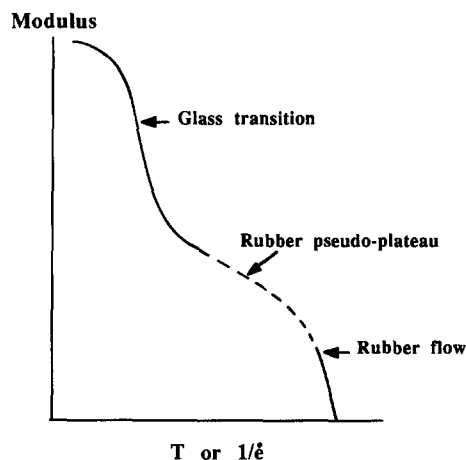


Figure 1 Typical temperature/time effects on the relaxation modulus of a polymer of low to moderate molecular weight. The viscoelastic region approximately corresponding to the experimental conditions in the present study is indicated by the broken line

superimposed. At the end of drawing, the sample was immediately air-quenched by opening the furnace door. The nominal strain rates used were 2.08, 0.417 and 0.0104 s^{-1} .

The specimen geometry of the undrawn film is shown in *Figure 2*, together with the horizontal and vertical lines used to characterize the deformation. During extension, the segments near the vertical edge of the film become narrow, whereas the centre segments maintain their initial width. Microstructure characterization was carried out only on the segments drawn at constant width, which is a pure shear deformation. Values of stress (in the draw direction) were obtained from the load–extension curves at the various draw ratios.

Density and crystallinity

The density ρ of the film specimens was measured at 23°C in a density gradient column containing n-heptane and carbon tetrachloride. The volume fraction crystallinity was estimated from

$$\chi = \frac{(\rho - \rho_a)}{(\rho_c - \rho_a)} \quad (1)$$

with the crystalline density $\rho_c = 1457 \text{ kg m}^{-3}$ and the amorphous density ρ_a taken as the measured density of the undrawn film. It cannot be assumed that ρ_c remains constant, but measurement of lattice spacings by X-ray diffraction indicates that it does for the range of deformation conditions applied in this study. Since our intrinsic polarized fluorescence studies³⁶ show that amorphous orientation in the drawn films did not exceed 0.45, changes in ρ_a due to drawing are expected to be negligible^{37–39}.

Crystallite size from wide-angle X-ray scattering

Wide-angle X-ray scattering (WAXS) analysis was performed with a Philips diffractometer in the transmission mode, using crystal-monochromatized $\text{CuK}\alpha$ radiation. Equatorial scans were made in the range $8\text{--}40^\circ$, with intensity data collected every 0.1° for a period of 10 s. A mathematical profile-fitting procedure was used to obtain peak ‘half-widths’ (full width at half peak maximum) for calculation of crystallite size. The procedure is similar to that devised by Heuvel *et al.*⁴⁰,

in which each of the four equatorial reflections (010, $\bar{1}10$, 100, and amorphous) is described by a Pearson VII function.

Specimens drawn at constant width lack cylindrical symmetry because the crystallites have planar as well as axial orientation, with the 100 planes tending to align parallel to the film surface. To measure the half-width of the 010 and 100 reflections reliably, therefore, two equatorial scans must be made: one in which the X-ray beam is incident on the film surface (through direction), and the other in which it is incident on the film edge. For the through direction, an intensity profile is obtained in which the 010 reflection is predominant (*Figure 3a*), whereas in the edge direction, the 100 reflection has

Table 1 Details of the PET films

Supplier	\bar{M}_n	Density (kg m^{-3})	Thickness (mm)
Rhône Poulenc	19 000	1339	0.147
Goodyear	21 000	1337	0.253
Goodyear	27 000	1336	0.253

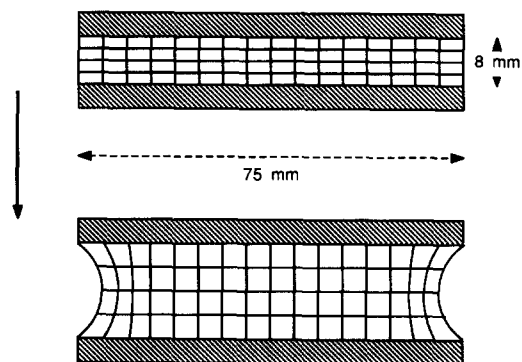


Figure 2 Specimen geometry of PET film, before and after drawing. Only the segments deformed at constant width were used in subsequent analysis

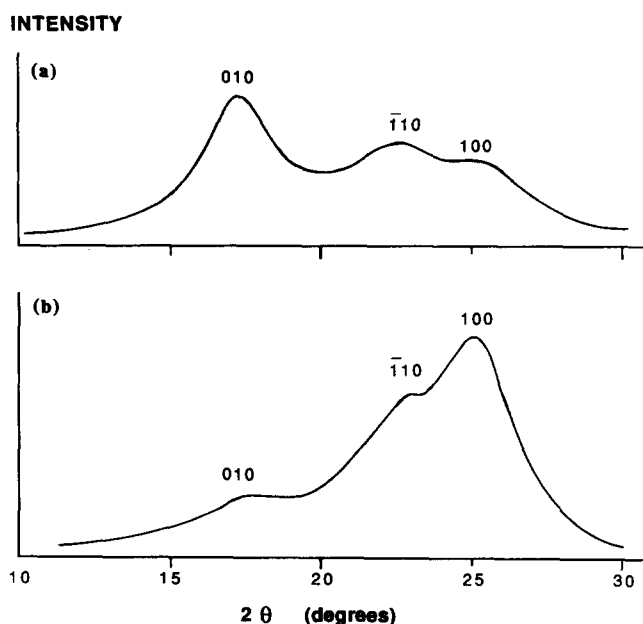


Figure 3 Equatorial WAXS scans of drawn PET film, with the X-ray beam incident on (a) the film surface (the through direction) and (b) the film edge (the edge direction)

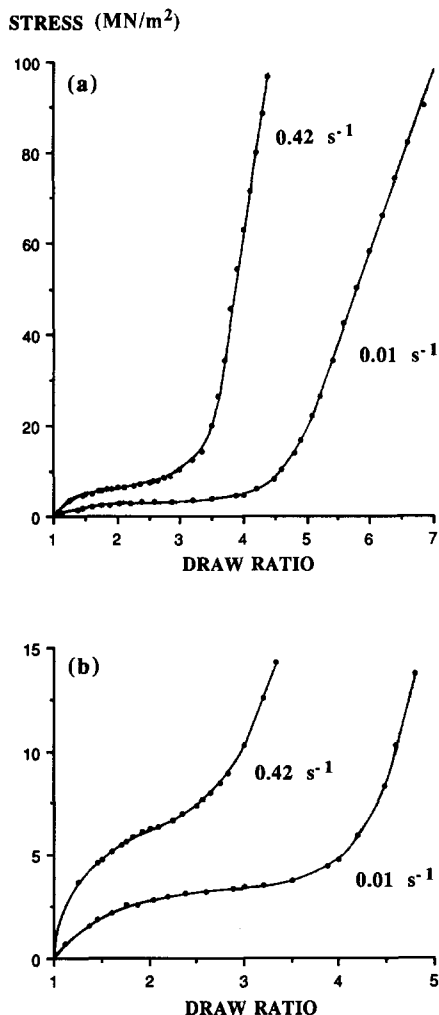


Figure 4 Influence of strain rate on the true stress versus draw ratio relationship for PET film drawn at 90°C: (b) enlarges the low stress region of (a)

the highest intensity (Figure 3b). The profile-fitting procedure was applied to both scans, since the half-width of the 010 reflection can be most accurately obtained from the through direction, and the 100 half-width from an edge scan.

Crystallite dimensions normal to the 010 and 100 planes were thus obtained using the Scherrer equation⁴¹ after correcting the peak half-widths for instrumental broadening. There is always the possibility of lattice distortion contributing to line breadth, but due to lack of suitable higher order reflections, the extent of this effect, if any, could not be investigated. Since in the present study we are concerned only with first-order reflections, the contribution of lattice distortion to line breadth is likely to be small.

Specimens for WAXS analysis in the through direction were prepared by cutting segments (12 mm × 8 mm) from the centre region of the drawn film, and stacking them to form a closely packed laminate 0.5 mm thick. Specimens to be analysed in the edge direction were made by cutting 'through-specimens' into 0.5 mm strips and restacking them to form a laminate about 8 mm wide and 0.5 mm thick. Glue was used only on the top and bottom edges of the laminates, outside the range of the X-ray beam.

RESULTS AND DISCUSSION

Crystallization and crystal growth

Drawing of amorphous, unoriented PET film generates stress-strain curves which depend on strain rate and drawing temperature. Figure 4 shows true stress versus draw ratio λ for two of the strain rates studied, at a draw temperature of 90°C. There is an initial low stress region followed by a pronounced increase in stress. Decreasing strain rate delays the onset of the upturn, and at strain rates somewhat lower than 0.01 s⁻¹ the polymer flows to failure with no upturn occurring. These are expected phenomena, which have also been observed by others^{12,25}. Relationships between structure formation during drawing and stress-strain behaviour will be discussed later, after presenting the results from microstructure characterization.

To monitor the development of crystallinity during drawing, film density was measured at different draw ratios (Figure 5). As has been observed before, lower strain rates delay the onset of crystallization to higher draw ratios and reduce the rate at which crystallinity increases with draw ratio. These effects arise from the greater time available for relaxation of orientation during drawing^{10,36}. Our study, however, reveals two crystallization regimes: in the first regime, crystallinity develops more rapidly than in the second, and, at all strain rates, the change in crystallization rate occurs at a similar crystallinity level (~15%). The two-stage nature of the crystallization process was not revealed in previous studies¹⁰, probably because the experiments did not involve such high strain rates or such high draw ratios (at lower strain rates).

For the constant extension rate experiment, we have not found any data in the literature showing crystallinity as a function of the stress developed during drawing. To do so, however, can simplify matters, as shown in Figure 6a, where crystallinity is plotted as a function of the final stress level in the drawn film. It is apparent that crystallinity could almost be considered a single function of true stress, with little visible influence of strain rate. A closer examination of the data does however reveal some significant strain-rate dependence. By enlarging the low stress region of the plots (Figure 6b), it becomes apparent that the critical stress for induction of

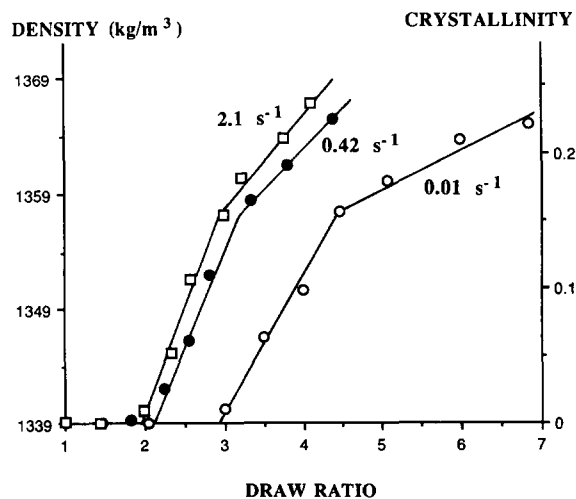


Figure 5 Variation of density and crystallinity with draw ratio λ at three strain rates

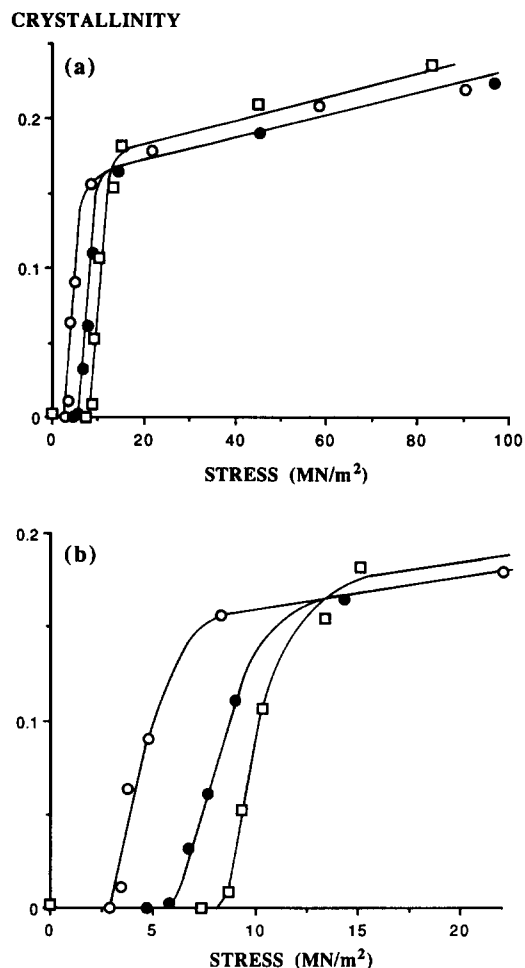


Figure 6 Crystallinity versus true stress for strain rates of 0.01 (○), 0.42 (●) and 2.1 s⁻¹ (□): (b) enlarges the low stress region of (a)

crystallinity increases with increasing strain rate. This result is consistent with our observation, presented elsewhere⁴², that at higher strain rates, higher stresses are required to reach the critical amorphous orientation for induction of crystallization.

In any case, Figure 6 confirms the existence of two crystallization regimes and helps to elucidate their nature. In regime 1, crystallization is initiated at a stress level in the region 3–8 MN m⁻², and only small stress increments are required to increase crystallinity from zero to ~15%. An abrupt change in slope in the stress range 7–12 MN m⁻² characterizes the onset of the second regime: in regime 2, large increments of stress produce small increases in crystallinity. We shall sometimes refer to regimes 1 and 2 as the low stress crystallization regime and the high stress crystallization regime, respectively. To obtain more detailed information about microstructural development in these regimes, WAXS was used to determine crystallite width in two crystallographic directions – normal to the 010 and 100 planes. These crystallite dimensions are essentially perpendicular to the chain axis. It is well known that in pure shear deformation (constant width drawing), the 100 planes tend to align parallel to the film surface³⁴.

It is evident from Figure 7 that crystallite width normal to the 010 planes increases significantly as a function of λ , and that the rate of growth is higher at the higher strain rates. Normal to the 100 planes, crystallite width

increases relatively weakly as a function of λ at the higher strain rates, and at the lower strain rate, this crystallite dimension is essentially independent of λ , appearing to have reached some kind of equilibrium size. Clearly, stress-induced crystal growth is asymmetric, with preferential growth occurring normal to the 010 planes. A similar observation has been made in the case of PET fibres^{38,42} and PET film drawn in simple extension⁴², and it is attributable to the existence of stronger molecular interactions between the 010 planes than between the 100 planes³⁸.

It is important to notice that essentially all our crystallite size data are in regime 2. Although weak crystalline reflections were observable in the WAXS scans, crystallite size could not be measured reliably in regime 1 due to high amorphous scattering. It is therefore uncertain whether crystallization in regime 1 involves monotonic crystal growth from nuclei formed prior to, or in the early stages of, regime 1; or whether it involves rapid formation of crystallites of 2–3 nm width on nuclei which are continuously forming as the stress increases. In the latter case, crystallization would mainly involve an increase in the number of crystallites per unit volume during deformation, and in the former case the size of the crystallites would increase, with relatively little change in their number density.

Figure 8 reveals the stress-dependent nature of crystal growth in regime 2. It is apparent that crystallite width at the onset of regime 2 is influenced by strain rate,

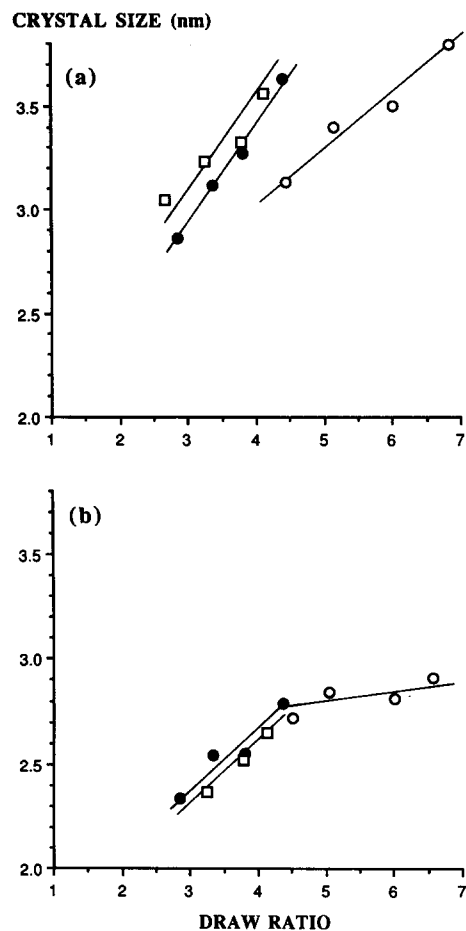


Figure 7 Crystallite width normal to (a) the 010 planes and (b) the 100 planes versus draw ratio λ . Strain rates are 2.1 (□), 0.42 (●) and 0.01 s⁻¹ (○)

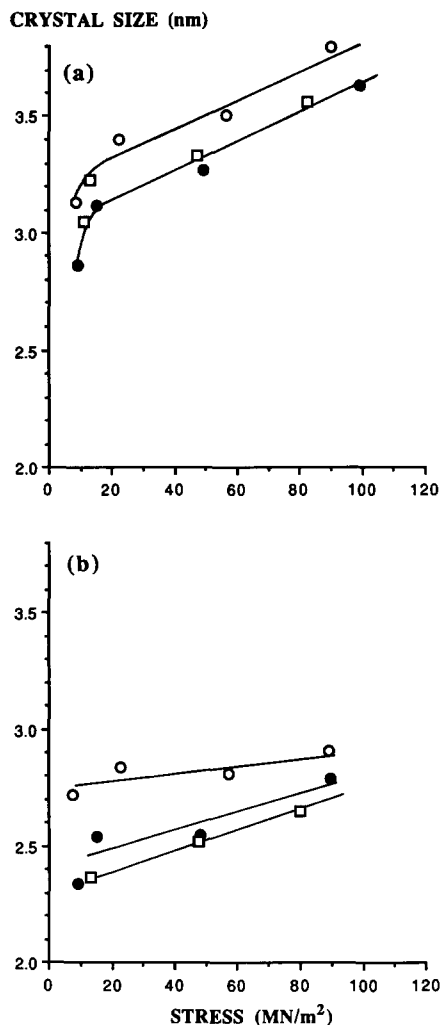


Figure 8 Crystallite width normal to (a) the 010 planes and (b) the 100 planes versus true stress. Strain rates are 2.1 (\square), 0.42 (\bullet) and 0.01 s⁻¹ (\circ)

especially normal to the 100 planes. One can argue that at lower strain rates, the greater time available for crystallization in regime 1 gives rise to larger lateral dimensions at the onset of regime 2. Since the level of crystallinity at the onset of regime 2 is about the same at all strain rates, this implies that at the low strain rate, there are fewer crystallites per unit volume and/or smaller crystallite dimensions in, for example, the chain axis direction. We are currently attempting to obtain reliable crystallite size measurements along the chain axis, although various experimental difficulties are involved. For the present, we can infer that the lateral crystallite dimensions are enhanced by high stresses and low strain rates. Further examination of the influence of draw time on crystal growth is given in the following paper⁴³.

Stress-strain-structure relationships

Relationships between structure evolution during hot-drawing of PET and stress-strain behaviour are not well understood. For example, since PET is not chemically crosslinked but does crystallize, one might attribute the upturn in stress to the crosslinking and reinforcing effect of crystallites. However, the precise point on the stress-strain curves at which crystallization is initiated has not been previously reported.

From our data, it is now possible to pinpoint the stress and draw ratio coordinates at which crystallization is initiated, E_1 , and at which the second crystallization regime begins, E_2 (Figure 9). It is interesting to observe that, at all strain rates, the onset of crystallization occurs at the inflection point in the stress versus draw ratio curve, and that the onset of regime 2 occurs in the region of the pronounced increase in gradient. This is perhaps more dramatically illustrated by a Mooney-Rivlin plot (Figure 10): a distinct decrease in slope occurs at the onset of crystallization, and the onset of regime 2 coincides with the starting point of the sharp upturn in reduced stress.

Our present interpretation of these results is as follows. There is a precrystallization regime involving deformation of an entanglement network, followed by two crystallization regimes which significantly influence stress-strain behaviour. The onset of crystallization causes an inflection point in the stress-strain curve, and the low stress crystallization regime involves the formation of a crystallite network. At a characteristic level of crystallinity ($\sim 15\%$), the crystallites have formed a network which is sufficiently effective to increase dramatically the stress required to deform the polymer. This results in a high stress crystallization regime, involving growth of existing crystallites and the deformation of a network in which crystallites are the predominant junction points.

This interpretation clearly involves some assumptions about cause and effect. For example, it could be argued that the onset of crystallization might not cause the

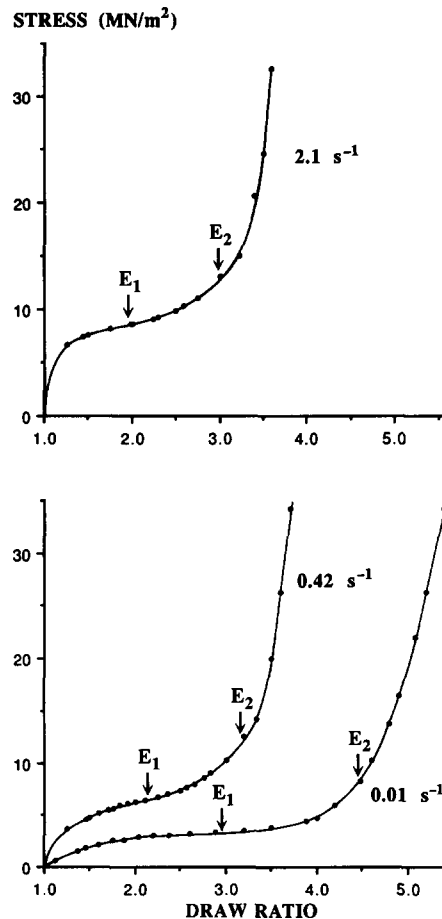


Figure 9 True stress versus draw ratio at three strain rates. The onset of crystallization, E_1 , and the onset of regime 2 crystallization, E_2 , are indicated

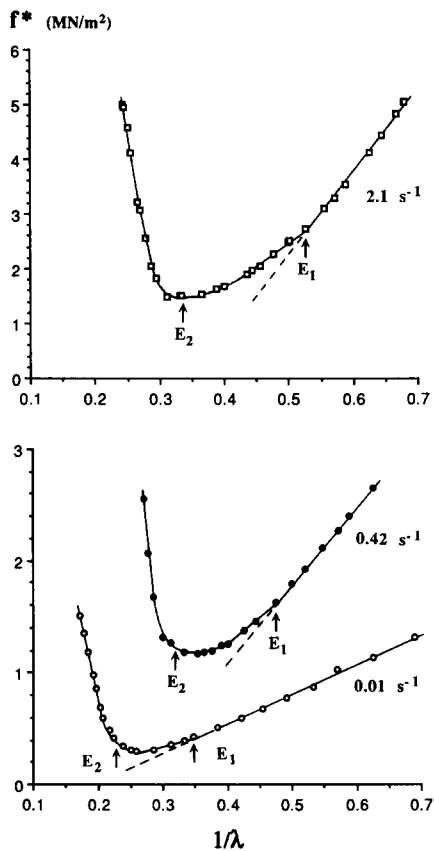


Figure 10 Reduced stress versus λ^{-1} at three strain rates. The onset of crystallization, E_1 , and the onset of regime 2 crystallization, E_2 , are indicated

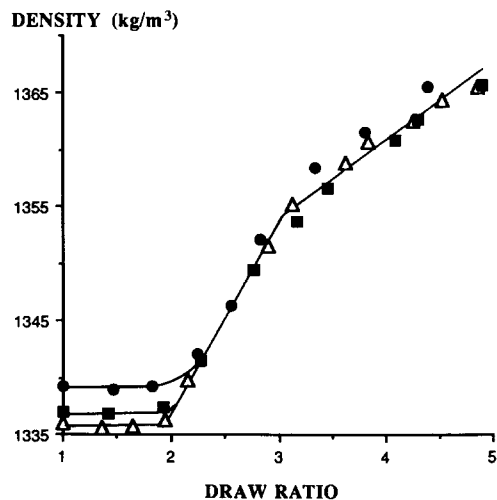


Figure 11 Density versus draw ratio, at a strain rate of 0.42 s^{-1} , for films of different molecular weights. $\bar{M}_n = 19\,000$ (●), $21\,000$ (■) and $27\,000$ (△)

inflection point in the stress–strain curve. The inflection could arise from reaching the limiting extensibility of the entanglement network, which might cause crystallization. However, the applicability of ‘limiting extensibility’ to PET deformed above T_g to high extensions seems doubtful. At high extensions, the entanglements are likely to slip and redistribute stress, rather than form tight knots. Further investigation of these questions is a continuing aspect of our research on PET, and will be discussed in greater detail elsewhere⁴⁴.

Influence of molecular weight

It would be pertinent to question whether the phenomena we have reported here are applicable to amorphous PET film in general, or whether the material we have studied might be atypical. Figure 11 shows density versus draw ratio for three different PET films. The Rhône Poulenc film, which was used in all the studies we have reported so far, has a thickness of 0.15 mm and a \bar{M}_n of 19 000. The Goodyear films are both 0.25 mm thick and have number average molecular weights of 21 000 and 27 000. All the films are unfilled and of high clarity. Despite the differences in molecular weight, film thickness, and, presumably, polymerization conditions, it can be seen that for the strain rate of 0.42 s^{-1} , the data for all three films are very close. The only significant differences occur in the precrystallization regime, because the density of the undrawn Rhône Poulenc film is 1339 kg m^{-3} whereas the densities of the undrawn Goodyear films are 1336 and 1337 kg m^{-3} . However, if we take these values as the true ρ_a values of the films and calculate crystallinity from equation (1) accordingly, a plot of crystallinity versus draw ratio (Figure 12a) shows that the data for all three films virtually coincide at all draw ratios. We can certainly conclude that the two-stage crystallization behaviour is of general applicability to the deformation of PET film.

CRYSTALLINITY

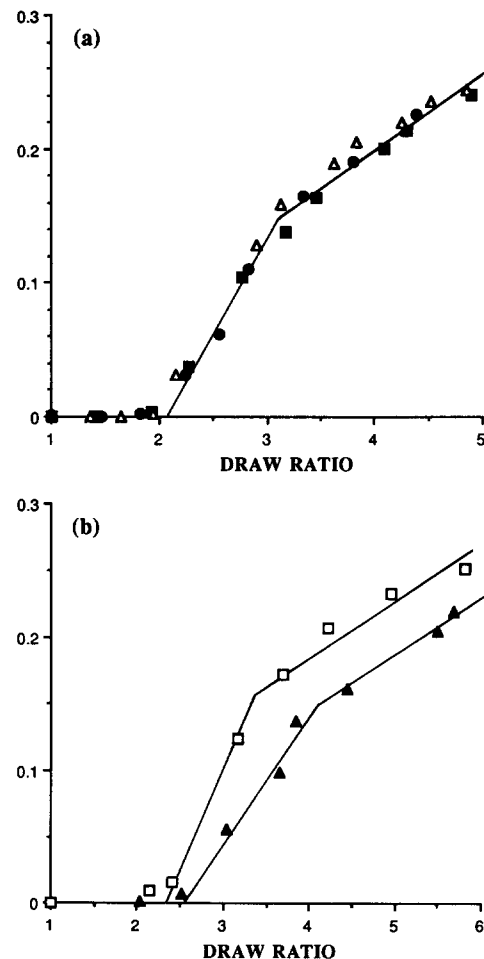


Figure 12 Influence of molecular weight on the crystallinity versus draw ratio relationship at strain rates of: (a) 0.42 s^{-1} , with $\bar{M}_n = 19\,000$ (●), $21\,000$ (■) and $27\,000$ (△); (b) 0.02 s^{-1} , with $\bar{M}_n = 19\,000$ (▲) and $27\,000$ (□)

We have also investigated the influence of molecular weight at a lower strain rate. *Figure 12b* shows crystallinity versus draw ratio for the films of highest and lowest molecular weight at a strain rate of 0.02 s^{-1} . Again, the two crystallization regimes are evident for both films, but it is apparent that crystallinity is induced at a lower draw ratio in the high molecular weight film. This probably reflects lower rates of molecular relaxation for higher molecular weights; the delay in the onset of crystallization with decreasing strain rate is smaller in the high molecular weight film, due to reduced relaxation of orientation during drawing. A more detailed study of molecular weight effects is underway.

CONCLUSIONS

During drawing of PET film at 90°C , the onset of crystallization always coincides with the inflection point in the stress-strain relationship, and shifts to higher draw ratios and lower stress levels as strain rate decreases. The extent of the draw ratio shift appears to be reduced by increasing molecular weight, reflecting a lower rate of molecular relaxation.

Crystallization proceeds in two regimes: a low stress regime (regime 1) in which stress increases slowly with draw ratio, and crystallinity increases relatively fast; and a high stress regime (regime 2) in which stress increases rapidly and crystallinity increases slowly. The onset of regime 2 occurs at a characteristic level of crystallinity, which is independent of strain rate. We speculate that regime 1 involves the formation of a crystallite network which, at the characteristic crystallinity level, becomes sufficiently effective to increase dramatically the stress generated during drawing.

The high stresses in regime 2 induce modest increases in crystallite width normal to the 010 and 100 planes, with preferential growth occurring normal to 010. Growth normal to the 010 planes has a stronger dependence on the level of strain (and stress) than 100 growth. For the latter, the time available for crystallization seems to play a more significant role.

ACKNOWLEDGEMENTS

These studies were undertaken in connection with the TRI project 'Structure and Properties of Poly(ethylene Terephthalate) Film', supported by a group of Corporate TRI Participants. The author is indebted to Lei Zhang and Dennis W. Briant for their careful experimental work, and to Dr H.-D. Weigmann for his encouragement.

REFERENCES

- 1 Alfonso, G. C., Verdoni, M. P. and Wasiak, A. *Polymer* 1978, **19**, 711
- 2 Smith, F. S. and Steward, R. D. *Polymer* 1974, **15**, 283
- 3 Gupte, K. M., Motz, H. and Schultz, J. M. *J. Polym. Sci., Polym. Phys. Edn* 1983, **21**, 1927
- 4 Brogato, G. and Gianotti, G. *Eur. Polym. J.* 1983, **19**, 803
- 5 Sun, T., Pereira, J. R. C. and Porter, R. S. *J. Polym. Sci., Polym. Phys. Edn* 1984, **22**, 1163
- 6 Peszkin, P. and Schultz, J. M. *J. Polym. Sci., Polym. Phys. Edn* 1986, **24**, 2591
- 7 Desai, P. and Abhiraman, A. S. *J. Polym. Sci., Polym. Phys. Edn* 1988, **26**, 1657
- 8 Desai, P. and Abhiraman, A. S. *J. Polym. Sci., Polym. Phys. Edn* 1989, **27**, 2469
- 9 Biangardi, H. J. and Zachmann, H. G. *J. Polym. Sci., Polym. Symp.* 1977, **58**, 169
- 10 LeBourvellec, G., Monnerie, L. and Jarry, J. P. *Polymer* 1986, **27**, 856
- 11 LeBourvellec, G., Monnerie, L. and Jarry, J. P. *Polymer* 1987, **28**, 1712
- 12 Spruiell, J. E., McCord, D. E. and Beuerlein, R. A. *Trans. Soc. Rheol.* 1972, **16**, 535
- 13 Flory, P. J. *J. Chem. Phys.* 1947, **15**, 397
- 14 Krigbaum, W. R. and Roe, R. J. *J. Polym. Sci. A* 1964, **2**, 4391
- 15 Andrews, E. H. *Proc. R. Soc. (London) A* 1964, **277**, 562
- 16 Andrews, E. H., Owen, P. J. and Singh, A. *Proc. R. Soc. (London) A* 1971, **324**, 79
- 17 Gent, A. N. *Trans. Faraday Soc.* 1954, **50**, 521
- 18 Peterlin, A. *Polym. Eng. Sci.* 1976, **16**, 126
- 19 Yeh, G. S. Y. *Polym. Eng. Sci.* 1976, **16**, 138
- 20 Yeh, G. S. Y. *Polym. Eng. Sci.* 1976, **16**, 145
- 21 Yeh, G. S. Y. and Hong, K. Z. *Polym. Eng. Sci.* 1979, **19**, 395
- 22 Yeh, G. S. Y., Hong, K. Z. and Krueger, D. L. *Polym. Eng. Sci.* 1979, **19**, 401
- 23 Keller, A. and Machin, M. J. *J. Macromol. Sci. Phys.* 1967, **B1**, 41
- 24 Keller, A. and Willmouth, F. M. *J. Macromol. Sci. Phys.* 1972, **B6**, 493
- 25 Thompson, A. B. *J. Polym. Sci.* 1959, **34**, 741
- 26 Yeh, G. S. Y. and Geil, P. H. *J. Macromol. Sci. Phys.* 1967, **B1**, 251
- 27 Koenig, J. L. and Hannon, M. J. *J. Macromol. Sci. Phys.* 1967, **B1**, 119
- 28 Misra, A. and Stein, R. S. *J. Polym. Sci., Polym. Phys. Edn* 1979, **17**, 235
- 29 Casey, M. *Polymer* 1977, **18**, 1219
- 30 Padibjo, S. R. and Ward, I. M. *Polymer* 1983, **24**, 1103
- 31 Dulmayer, W. J. and Geddes, A. L. *J. Polym. Sci.* 1958, **31**, 499
- 32 Heffelfinger, C. J. and Schmidt, P. G. *J. Appl. Polym. Sci.* 1965, **9**, 2661
- 33 Heffelfinger, C. J. and Lippert, E. L. *J. Appl. Polym. Sci.* 1971, **15**, 2699
- 34 Heffelfinger, C. J. and Burton, R. L. *J. Polym. Sci.* 1960, **47**, 289
- 35 Ravens, D. A. S. and Ward, I. M. *Trans. Faraday Soc.* 1961, **57**, 150
- 36 Clauss, B. and Salem, D. R. *Polymer* 1992, **33**, 3193
- 37 Nobbs, J. H., Bower, D. I. and Ward, I. M. *Polymer* 1976, **17**, 25
- 38 Huisman, R. and Heuvel, H. M. *J. Appl. Polym. Sci.* 1978, **22**, 943
- 39 Heuvel, H. M. and Huisman, R. *J. Appl. Polym. Sci.* 1978, **22**, 2229
- 40 Heuvel, H. M., Huisman, R. and Lind, K. C. J. B. *J. Polym. Sci., Polym. Phys. Edn* 1976, **14**, 921
- 41 Cullity, B. D. 'Elements of X-ray Diffraction', Addison-Wesley Inc., London, 1967, Ch. 3, pp. 96-99
- 42 Salem, D. R. in preparation
- 43 Salem, D. R. *Polymer* 1992, **33**, 3189
- 44 Clauss, B. and Salem, D. R. in preparation